Materials Science in Semiconductor Processing 199 (2025) 109864

Contents lists available at ScienceDirect

Materials Science in Semiconductor Processing

journal homepage: www.elsevier.com/locate/mssp

Theoretical calculation of size- dependent properties and the impact of carbon doping on lithium titanate oxide nanoparticles as anode material in Li-ion batteries

Abdul Majid [a,*], Fiza Shafique [a], Sawaira Tasawar [a], Mohammad Alkhedher [b], Salah Ud-Din Khan [c], Kamran Alam [d], Sajjad Haider [e]

[a] Department of Physics, University of Gujrat, Gujrat, 50700, Pakistan
[b] Mechanical and Industrial Engineering Department, Abu Dhabi University, Abu Dhabi, 59911, United Arab Emirates
[c] College of Engineering, King Saud University, P.O.Box 800, Riyadh, 11421, Saudi Arabia
[d] VITO (Flemish institute for Technological Research), Separation and Conversion Technology, Boeretang 200, 2400, Mol, Belgium
[e] Chemical Engineering Department, College of Engineering, King Saud University, P.O.Box 800, Riyadh, 11421, Saudi Arabia

ARTICLE INFO

Keywords:
Lithium titanate oxide (LTO)
Density functional theory (DFT)
Lithium-ion batteries (LIBs)
Ab-initio molecular dynamics (AIMD)
Anode

ABSTRACT

The technological improvement of lithium-ion battery (LIB) has been the center of research attention in the field of rechargeable batteries. This work reports investigation on prospects of lithium titanate oxide (LTO) nanoparticles as anode material in LIB via density functional theory and ab-initio molecular dynamics (AIMD) stimulations. The first study on effects of size variation and doping of carbon via AIMD simulations in LTO nanoparticles is studied here to explore the anodic properties of the material on the basis of structural properties, electronic characteristics, thermal stability, storage capacity, lithiation energy, and diffusion kinetics. The doping appeared to increase the storage capacity of LTO from 175 $mAhg^{-1}$ to 1057 $mAhg^{-1}$ which points to practicality of the material as anode in LIBs. The open circuit voltage is found as 3.08 V, 3.40 V, 2.70 V and 0.70 V for 1.2 nm, 1.5 nm, 3.4 nm and carbon doped nanoparticles respectively. Cl-NEB simulations are carried out to study the migration paths of Li and vacancy in the host structure indicated low energy barrier of 0.86 eV for 1.2 nm, 0.75 eV for 1.5 nm and 0.45 eV for the doped structure, respectively. Furthermore, the MD simulations indicate the diffusion coefficient as $4.3x10^{-12}$ m^2/s, $5.0x10^{-12}$ m^2/s, $0.83x10^{-12}$ m^2/s and 1.72 $x10^{-8}$ m^2/s for 1.2 nm, 1.5 nm, 3.4 nm and doped 3.4 nm respectively. The calculated values of ionic conductivity of LIBs are 5.32 x 10^{-3} Sm^{-1}, 0.19 x 10^{-2} Sm^{-1}, 9.32 x 10^{-2} Sm^{-1} and 7.33 x 10^{-3} Sm^{-1} for 1.2 nm, 1.4 nm, 3.4 nm and doped 3.4 nm respectively.

1. Introduction

The global energy sector is undergoing a major transformation via replacement of fossil fuels with renewable and sustainable energy sources to fulfil the worlds energy demands [1,2]. The energy demand is estimated to increase by 50 % by 2050 due to which the production of high performance energy storage systems has become inevitable [3]. In this regard, rechargeable batteries are proved viable solutions to power the electronic devices and electrical vehicles. The commercially available metal ion batteries include LIBs, magnesium ion batteries (MIBs) and aluminium ion batteries (AIBs). The current technology related to LIBs offers up to 95 % discharge permissible making them suitable for energy storage device [4,5]. The versatility and low cost of LIBs make them a major contributor to the global clean energy revolution but with the surging demand of high performance anode materials, the existing limitations in LIB technology have also became more prominent (see Table 1).

The search of appropriate anode materials offering suitable physical, and chemical properties along with high storage capacity for use in multivalent batteries is still in progress. The currently available LIBs mostly rely on graphite anode which exhibits theoretical capacity of 372 $mAhg^{-1}$ which is deficient when future energy needs are taken into account [6]. The theoretical storage capacity of 4000 mAh/g has been reported in case of silicon based anode material in LIBs [7]. However, its

* Corresponding author.
E-mail address: abdulmajid40@yahoo.com (A. Majid).

https://doi.org/10.1016/j.mssp.2025.109864
Received 15 April 2025; Received in revised form 27 June 2025; Accepted 13 July 2025
Available online 21 July 2025

Table-1
Comparison of key parameters of emerging anode materials for battery applications.

Anode materials (Battery type)	Theoretical Specific Capacity (mAh/g)	Diffusion Barrier (eV)	Stability (DFT/ AIMD)	Reference
α-Graphyne (Na-ion)	279	0.23	High (AIMD)	[23]
P_5C_6 Monolayer (Na-ion)	590.5	0.019	High (AIMD)	[24]
B_2C Monolayer (K-ion)	796.9	0.07	High (AIMD)	[25]
B-doped Biphenylene (Li/Na-ion)	560.67 for Li 934.45 for Na	–	High (DFT)	[26]
Zr_2N MXene (Ca-ion)	1034	0.076	High (AIMD)	[27]
α-SiN (Li-ion)	956.16	0.30	High (AIMD)	[28]
α-SiP (Li-ion)	733.66	0.16	High (AIMD)	[28]

stability is compromised due to large volume expansion of about 400 % during the lithiation process which causes unaffordable mechanical degradation [8,9]. Similarly, the tin oxide-based anode materials have gained spotlight with high storage capacity of 790 mAh/g but its large volume changes during charging and discharging cycles cause early degradation which limits the stability of battery. The alternative materials like transition metal oxides, and niobium-based anode materials have also been inspected in this regard but despite their stability, the poor Coulombic efficiency, low conductivity, and scalability problems are yet to resolve [10-12]. The usage of SnO_2 nanoparticles in potassium ion batteries facilitated ionic transport in the electrolyte to produce the storage capacity of 231.7 mAh/g at 1 A/g after 400 cycles [13]. The utilization of $SrRuO_3$ and B_4C_3 as an anode in multivalent-ion batteries has exhibited excellent transport characteristics with high capacity but high costs due to fabrication issues make it economically challenging for use in practical applications [14-16].

The conventional anode materials used in LIBs exhibit various challenges including limited cycle life, thermal runaway, and lithium plating at high charging rates, which restrict the electrochemical performance of the battery. In order to overcome these challenges, more focused research efforts are needed to obtain high-performance anode materials. Among all the promising anode candidates, lithium titanate oxide ($Li_4Ti_5O_{12}$) has grabbed attention owing to its unique properties including "zero-strain" characteristic during lithiation and delithiation which ensures exceptional structural stability and long cycle life [17]. These properties enable $Li_4Ti_5O_{12}$ (known as LTO) to endure thousands of cycles without major decay while the traditional graphite anode is prone to degradation over time. In addition to that, the higher operating voltage (1.55 V vs. Li^+/Li) of LTO alleviates the risk of lithium plating making it suitable for large-scale applications and reducing the chances of thermal runaway [18].

The high rate capability of LTO makes its way into applications like electric vehicles and grid energy storage systems by providing extremely fast charging and high-power delivery [19]. The capability of LTO to perform in both high-temperature and low-temperature environments makes it more appealing than traditional graphite, which exhibits slow kinetics at low temperatures and decomposition of electrolyte at high temperatures. The durable spinal structure of LTO demonstrates its compatibility with multivalent ions (e.g. Zn^{+2}, Al^{+3}, and Mg^{+2}), making it potential candidate for future multivalent ion batteries [20]. Moreover, the significant improvement in coulombic efficiency of LTO is primarily attributed to the reduction in the formation of solid-electrolyte interface (SEI) layer. Futhermore, LTO is advantageous due to its non-toxic nature from the environmental and economic perspective and longer lifespan which provide low maintenance benefit and longer service life that compensate its initial higher cost. By combining these characteristics with high power density and minimal volume expansion during charging and discharging cycles, LTO is an ideal choice for high-performance, low maintenance and fast charging applications offering added stability and safety features [21]. However, despite the mentioned attractive material features, the LTO based anode faces challenges due to its low electronic conductivity, moderate lithium-ion diffusion kinetics, and low theoretical capacity of 175 mAh/g [22].

The research activities are in progress to increase functionality of LTO by material modification strategies including doping, alloying, surface reconstrution, formation of nanoclusters of different sizes and morphology. DFT and AIMD calculations are helpful to predict and assess new competitors for high-performance anode materials beyond graphite and silicon. Recently, several efforts have been made in investigating two-dimensional (2D) materials, heterostructures, and doped materials for a variety of ion batteries such as lithium, sodium, potassium, magnesium, and calcium systems in order to increase specific capacities, reduce barriers to diffusion, and improve stability [23-28]. The development of new materials appeared to offer improved properties when compared to the conventional graphite and silicon. P_5C_6 and B_2C show low diffusion barriers and thus quicker charge/discharge rates [24,25]. In addition, many of these new materials maintain structural and thermal stability under operational conditions, which gives them an advantage over silicon, which undergoes large volume expansion. The comparison of key parameters of emerging anode materials is provided in the Table 2.

The doping of carbon in experimental settings has been found useful to optimize the electronic conductivity and stability to promote the charge transfer and prevent the agglomeration of particles [29-32]. In contrast, this work offers the dual staretegy of carbon doping and the reduction of size of LTO to nanoscale which helps in in shortening Li^+ diffusion pathways by increasing the electrode-electrolyte contact area [30,31,33-36]. LTO is spinel material which holds substantial market presence after graphite due to its good cycle, solidity, rate potentiality and protection not only with conventional but also with low temperature electrolytes [37]. It can be used as an excellent anode material whose structure can naturally sustain during the Li-intercalation and de-intercalation to ensure a long cycle stability [38]. Hence, the LTO based anode enhances the structural stability of multivalent batteries providing more intercalation potential than conventional graphite anode (0.1–0.2V against Li^+/Li) and prevents thermal runaway of the battery [39].

The pathways for optimizing the anode materials by understanding the role of size-dependence and doping on utilization of LTO can be exploited to improve the current status of LIBs. This research addresses a crucial gap in anode materials field by investigating the combine effect of doping and size reduction in LTO nanoparticles for use as anode in LIBs. The work involves comprehensive analysis of structural, electronic, and electrochemical properties of LTO nanoparticles via first principles-based calculations. The findings of this work highlight the

Table-2
The calculated parameters of the C doped LTO as anode material and comparison with literature.

Anode materials	Capacity (mAh/g)	Open circuit Voltage (V)	Energy barrier (eV)	Reference
C-$Li_4Ti_5O_{12}$ (for LIBs)	1057	0.70	0.45	Current work*
Green phosphorus (GP) (LIBs)	288.4	2.07	0.14	[60]
AlP (LIBs)	924	0.56	0.38	[61]
TiB_4 (LIBs)	2353.2	–	0.24	[62]
GeP_3 (LIBs)	648	0.4	0.5	[63]
Covalent triazine framework (LIBs)	925.99	0.51	0.65	[64]
TiC_3 (LIBs)	1916	0.26	0.25	[65]
WC_4 (LIBs)	577	0.65	0.55	[66]

potential of this approach to overcome the limitation of low storage capacity in the conventional anode materials, while offering new strategy to develop novel anode materials in LIBs. This study contributes to the existing knowledge to address the future demands related to dependable, sustainable, and more efficient energy storage tools.

2. Computational details

The work was carried out using Reaxff module of Amsterdam density functional (ADF) to examine $Li_4Ti_5O_{12}$ as an anode material for use in LIBs. The base material of LTO contained spinal-like framework with monoclinic structure and C2/c space group containing three inequivalent Li^+ sites with tetrahedral and octahedral coordination and three Ti^{4+} sites with octahedral coordination [40-42]. The unit cell of the base material was fully relaxed with 'none' periodicity and the optimized structure was converted into zero-dimensional supercell in the form of nanoparticles having size of 1.5 nm containing 84 atoms. The primitive unit cell containing 42 atoms was constructed by reducing the size of 1.5 nm–1.2 nm cluster and optimized using Reactive Force Field method to ensure the structural stability. Similarly, larger cluster of 3.4 nm in length was obtained by constructing the supercell having 672 atoms. The structure was optimized using convergence criteria 10^{-5} eV, gradient convergence criterion was 0.001 eV/Å while keeping the step convergence at 0.01 Å. The LTO was investigated in the form of nanoparticles having different sizes including 1.2 nm, 1.4 nm, 3.4 nm. The thermal stability of the nanoparticles was investigated via ab initio Molecular Dynamics (AIMD) simulations. A Nose-Hoover Chain thermostat with a step size of 0.25 fs and 100,000 steps was used in the AIMD arrangement. To maintain the total angular momentum of the system, the chain length was fixed at 10 with time constant of 0.5 fs over the temperature range of 300 K, 500 K, 700 K, and 900 K. The geometry optimization of the nanoparticles was performed to investigate the intercalation energies of Li-atoms at different symmetry sites via ensuring the exothermic conditions engaged in the intercalation of Li-atoms. Meanwhile, the energy involved in intercalating Li into the host material $Li_4Ti_5O_{12}$ nanoparticles is calculated using equation (1).

$$E_{intercalation} = E_{X_n\text{Li4Ti5O12}} - n \times E_X - E_{\text{Li4Ti5O12}} \quad (1)$$

The value $E_{intercalation}$ denotes the intercalation energy of Li atom placed into the host structure, $E_{X_n\text{Li4Ti5O12}}$ indicates the energy of intercalated host $Li_4Ti_5O_{12}$, X represents Li, n represents the number of Li atoms involved in simulations, and $E_{\text{Li4Ti5O12}}$ points to the optimized energy of the pure $Li_4Ti_5O_{12}$. Equation (1) can be used to determine the adsorption energy by systematically introducing the Li atoms into the host system. The reaction is considered favorable only if the adsorption energies show negative values indicating an exothermic reaction.

The storage capacity is calculated using equation-(2).

$$C_M = \frac{n^* z^* F}{M_{\text{Li4Ti5O12}}} \quad (2)$$

Where F represents Faraday's constant, n represents the number of Li atoms involved in the simulation, z indicates the valance number (z = 1 for Li), and $M_{\text{Li4Ti5O12}}$ denotes the mass of $Li_4Ti_5O_{12}$ in the denominator of the equation-(2).

The open circuit voltage (OCV) provides primary information for evaluating the electrochemical performance of any anode material. Equation-(3) is used to determine the value of OCV.

$$OCV \approx \frac{E_{X_{n2}\text{Li4Ti5O12}} - E_{X_{n1}\text{Li4Ti5O12}} - (n_2 - n_1)\mu_X}{z(n_2 - n_1)e} \quad (3)$$

Where $E_{X_{n2}\text{Li4Ti5O12}}$ and $E_{X_{n1}\text{Li4Ti5O12}}$ are the optimized energies associated with the intercalated host materials having n_2 and n_1 concentration of Li. μ_X, e and z denotes the chemical potential of guest atoms and electronic charge and the valence number (z = 1 for Li), respectively [43].

The energy barriers faced by the intercalating atoms in the host structure were computed by using the nudged elastic band (NEB) simulations which are used to model the diffusion process. This information is used to understand battery's charging and discharging rates. The intercalation processes insights were developed by examining the movement pathways of Li within the host structure. In order to model the Li migration diffusion procedure across the host material layers, the value of energy barrier was computed.

The energy required for Li to transverse the layers of host structure's is critical process to evaluate the charging efficiency of LIBs and different paths are pursued for Li atoms in this regard. During the Cl-NEB simulation, the spring constant is set at 1 Ha/Bohr^2 with a skewness value of 1. The energy criteria are set as 10^{-5} eV with a step convergence of 0.01 Å while the restart displacement is 0.05 Å. The force magnitude acting on the analyzed image is analyzed by using equation-(4) given below:

$$F_i = |F^s|_{\|} - |\nabla E(R_i)|_{\perp} \quad (4)$$

Where Fi indicates the overall force on the ith picture, $F_i^s \|$ represents the spring force, and $|\nabla E(R_i)|_{\perp}$ shows actual force. The state with the feasible energy is produced by Equation-(5),

$$R_i\,max = \nabla E(R_i\,max) + 2\nabla E|R_i\,max|_{\|} \quad (5)$$

In order to determine the diffusion coefficient, the molecular dynamics simulations are utilized while incorporating the Einstein relation which states that the self-diffusion coefficient of any atom moving randomly in three dimensions is determined via mean-square displacement (MSD) as a function of time. Equation-(6) and equation-(7) were used to determine the values of MSD and diffusion coefficient respectively.

$$Mean\ Square\ Displacement = \langle\ |r(t) - r(0)^2|\ \rangle \quad (6)$$

$$Diffusion\ coefficient = \frac{1}{6N}\lim_{t\to\infty}\frac{d}{dt}\sum_{t=1}^{N}\langle |ri(t) - ri(0)|^2\ \rangle \quad (7)$$

where the position vector of the atom at times t and t = 0 is indicated by the symbols r(t) and r(0), respectively. Equation-8 is used to calculate the ionic conductivity to study the charging rate.

$$\sigma = \frac{nq^2}{K_b T} D \quad (8)$$

where T is the temperature at which simulations are run, σ is the ionic conductance, q is the charge, D is the diffusion coefficient between 300K and 900 K, and K_b is the Boltzmann constant.

3. Results and discussion

The description of the findings on size-dependent electrochemical properties, effect of carbon doping on reaction kinetics and diffusion barrier in $Li_4Ti_5O_{12}$ for anodic applications is given in the coming sections.

3.1. Pure and carbon-doped lithium titanate oxide

The spinal structure $Li_4Ti_5O_{12}$ has a monoclinic phase with the space group C2/c and density of 3.50 gcm^{-3}. The optimized lattice parameters, a = 8.35 Å, b = 8.32 Å and c = 13.17 Å and calculated band gap 2.66 eV suggests that it is a semiconductor material [44,45]. First-principles calculations are carried out to determine the structural properties of $Li_4Ti_5O_{12}$ at the 0 D level [46] as depicted in Fig. 1, which reveals that Li and Ti atoms are bonded with O atoms. The structural impact on electrode material in LIBs is studied by considering the three structures of $Li_4Ti_5O_{12}$ of different sizes 1.2 nm (42 atoms), 1.5 nm (84 atoms) and 3.4 nm (672 atoms). The calculated bond length of Li-O is

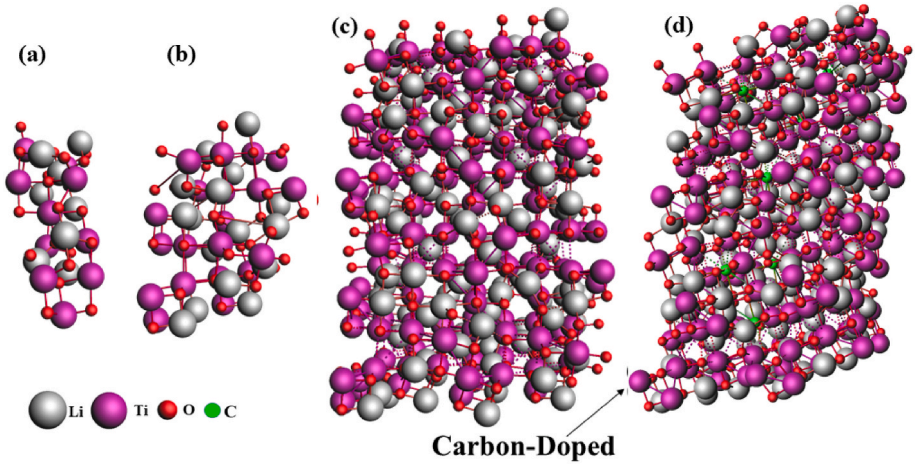

Fig. 1. The optimized nano-clusters of LTO shown along x-axis (a) 1.2 nm (b) 1.5 nm (c) 3.4 nm and (d) Carbon doped 3.4 nm.

165.60 p.m. (1.65 Å), the bond length of Ti-O is 157.60 p.m. (1.57 Å) and the bond length of Ti-Li is 276.81 p.m. (2.76 Å). The value of calculated dihedral bond angle Li-Ti-O is calculated as 91°. The calculated values of formation energies of the structures suggested that structures are stable.

We further investigated the LTO by increasing the size of the structure from 1.2 nm to 1.5 nm and then to 3.4 nm after which the structure remains stable as shown in figure-1. The $2 \times 2 \times 2$ supercell of $Li_4Ti_5O_{12}$ contains 672 atoms with size of 3.4 nm as shown in figure-1 with 128 Li atoms, 160 Ti and 384 O atoms with a volume of 871.1 $Å^3$. In the pure LTO supercell having 672 atoms, 5 % carbon doping is introduced to study the effects on the electrochemical performance of the structure. 8 carbon atoms are introduced on Ti cite (C_{Ti}) inside the supercell attempting to uniformly distributed the dopants in the cluster as shown in the figure-1. The carbon atom is introduced in larger cluster to ensure the structural integrity while gaining the benefits of electron donation from C atom. The carbon atoms can be uniformly distributed into 3.4 nm cluster while preserving the 'zero-strain' property of LTO and providing better kinetics and reducing diffusion barrier. The calculated bond length of Li-O is 1.96 Å, the bond length of C-O is 1.84 Å and the bond length of Ti-Li is equal to 1.58 Å. The calculated value of dihedral bond angle of Li-Ti-O is 91°. The calculated formation energy of the C_{Ti}-LTO structure is −6.36 eV/atom pointing to stability of the doped structure.

3.2. Thermal stability

The thermal stability of anode materials plays important role in the batteries as it sheds light on mechanism of heat transfer and overheating which may lead to thermal runaway [47]. High thermal stability helps indicates efficient dissipation of heat generated during battery operation, contributing to better overall performance and lifespan of the device. To evaluate the thermal stability of LTO, AIMD simulations were carried out at temperatures 900 K. The calculations employed on the host materials ran for 12 ps at a time step of 0.5 fs. The results showing temperature and energy plotted against time as shown in Fig. 2(a) which demonstrates that energy fluctuations are about 2.0 eV. Fig. 2(b) displays the structural snapshots obtained after 12 ps at 900 K which shows any absence of structural distortion or bond breakage, confirming that the structure of the material remains intact at high temperatures.

Moreover, rather than merely relying on DFT based energies to calculate the lithiation energy via equation (1), the AIMD simulations were performed to model the potential incorporation of Li atoms. The maximum numbers of Li in the host material determined by using equation (2) per the exothermic conditions helps modeling the optimal stoichiometric ratio required to maintain charge neutrality and structural stability. The intercalation of Li atoms in the host without any indication of metallic clustering and dendrite formation as per figure-3 (c) and (d) is valuable. Figure-3 (a)–(d) illustrate the energy and temperature stability of fully loaded structure over time during AIMD simulations conducted at 900 K for LIBs. Throughout the simulation the observed minimum system's energy changes points to thermal stability of the structure. Fig. 4(a)–4(d) show the host structure snapshots with 13Li atoms, 19Li atoms, 101Li atoms in the host $Li_4Ti_5O_{12}$ and 568Li atoms in the C doped $Li_4Ti_5O_{12}$ adsorbed following 12 ps of AIMD simulations 900 K, respectively.

The thermal endurance of LTO was checked by varying the temperature up to 900 K and the absence of abrupt energy spikes in Fig-3(a) to Fig. 3(d) indicates that LTO anode material can withstand the high-

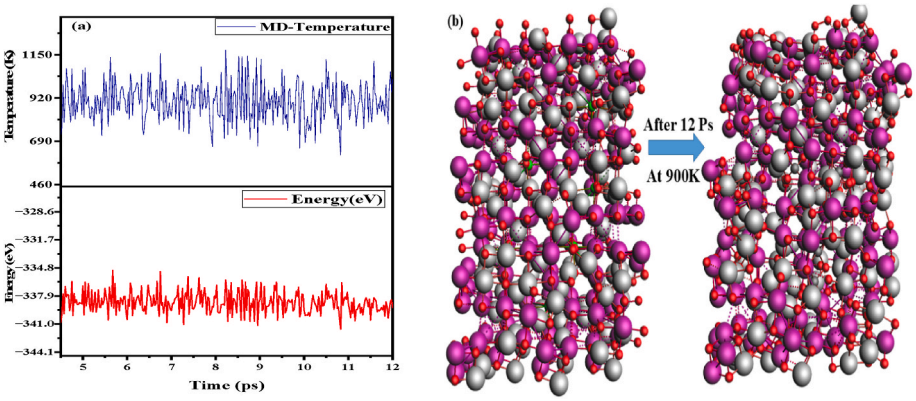

Figure-2. (a) Computed AIMD simulations illustrating how energy changes with temperature (b) The LTO structural snapshot at 900 K, taken before and after 12 ps.

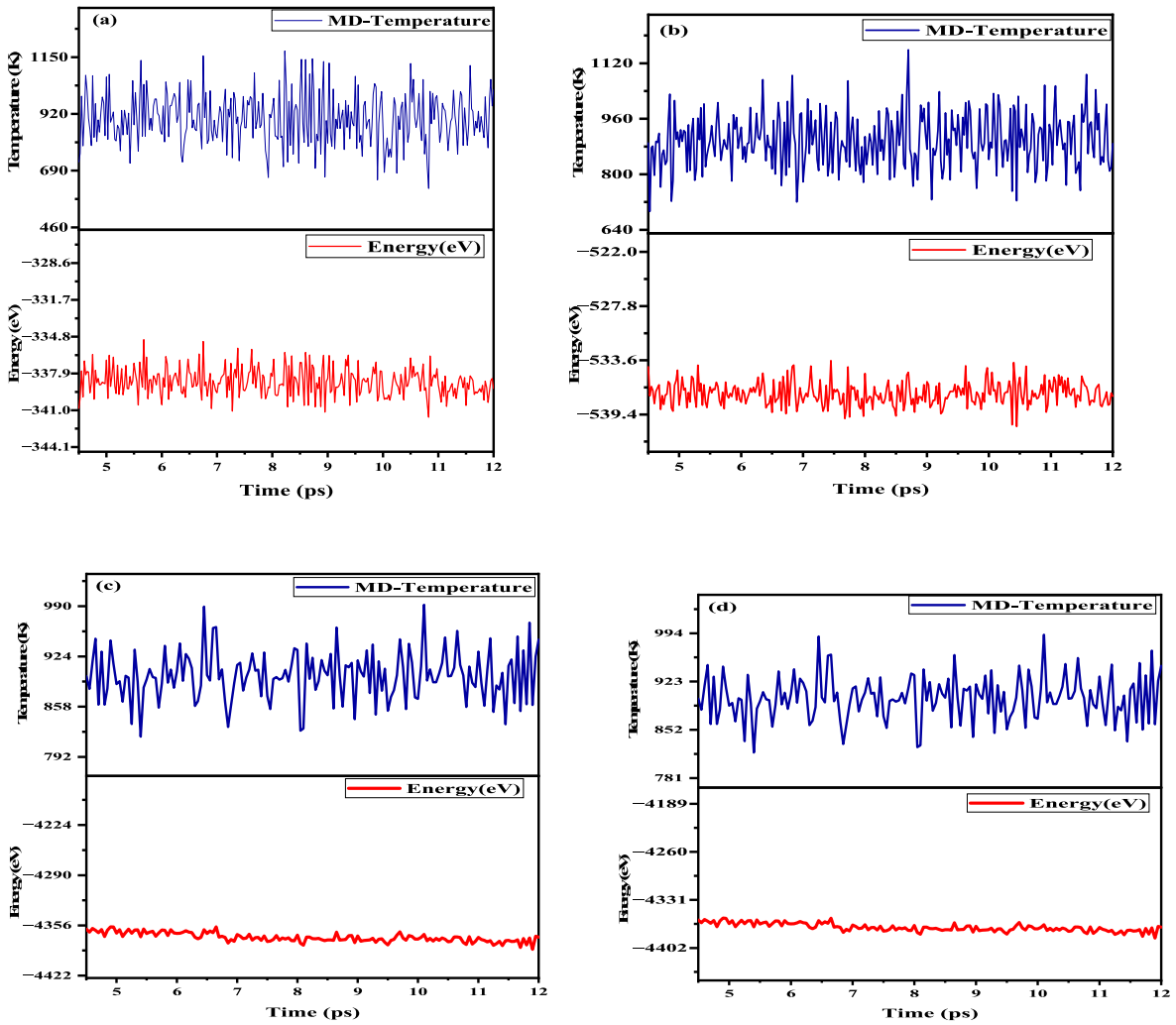

Figure-3. AIMD calculations representing the change in the temperature and energy with time for (a) intercalated 13Li atoms (b) intercalated 19Li atoms (c) intercalated 101Li atoms in the Pure $Li_4Ti_5O_{12}$ and (d) adsorbed 568Li atoms in the host C- $Li_4Ti_5O_{12}$.

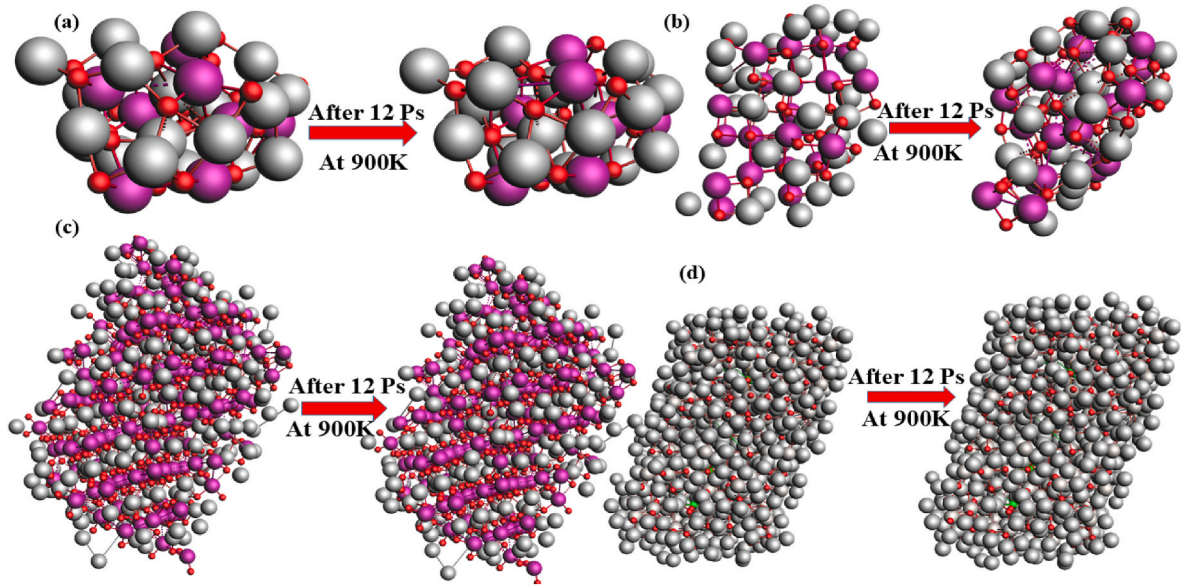

Figure-4. The snapshot of the host taken at 900 K before and after the AIMD simulation with (a) 13 Li atoms and (b) 19 Li atoms (c) 101 Li atoms in pure LTO and 568 Li atoms in the host C- LTO.

temperature conditions. The material is stable even at high temperature due to its zero-strain characteristics and negligible volume changes during charging and discharging process making it ideal choice for battery applications. The reliability of the computational setup is ensured by keeping the time step of 0.5 fs which captures the high frequency atomic motions while remaining efficient hence providing LTO a rigid framework which is resistant to the thermal degradation. Similarly, minor structural changes with minimum bond breakage are observed in Fig-4 which indicates that the LTO is an ideal material for its applications in high temperature energy storage systems.

3.3. The adsorption energies of Li intercalated LTO

The addition of Li atoms into the host LTO is investigated to model the charge/discharge cycles of LIBs [48]. The lithiation energy refers to the energy obtained after placing Li-ions in the host as a crucial process in batteries. The adsorption energies for Li atoms intercalated into the host material is studied for all LTO nanostructures to determine the interaction between the intercalants and host atom to monitor whether the reaction is exothermic or endothermic. The adsorption energy is calculated via equation (1) which indicates gradual rise with the number of intercalating as depicted in Fig. 7(a). Firstly, the value of lithiation energy is computed for 1.2 nm LTO by positioning different numbers of Li atoms at various sites in the host structure. We find out the lithiation energy exhibits exothermic reaction until the intercalation of 13 Li atoms takes place in the host as shown in Fig. 5(a). The further intercalation indicates that the subsequent Li moves away from the structure and thus the insertion of 14^{th} Li atom switched the reaction to endothermic as seen in figure-6(a). Secondly, the intercalation of Li atoms into the 1.5 nm LTO is modeled by arranging varying quantities of Li atoms at different locations inside the host structure. The calculated values indicate that the process remains exothermic up to intercalation of 19 Li atoms into 1.5 nm LTO as shown in figure-5(b). However, the process turns endothermic upon intercalation of 20^{th} Li atom into the host structure as depicted in figure-6(b) according to which the next Li goes away from the structure indicating the host's inability to adsorb the further intercalants.

Thirdly, the lithiation energy for 3.4 nm LTO is determined different configurations of placing Li atoms at various points inside the host structure as shown in Fig. 5(c). The calculated values show that lithiation process remains exothermic up to insertion of 101 Li atoms inside the host. The reaction becomes endothermic upon insertion of 102^{nd} Li atom into the host structure as shown in figure-6(c) according to which the further intercalant goes away from the structure depicting the material's limits of hosting the Li atoms.

The lithium intercalation in the host C-LTO structure is shown in Fig. 5(d) according to which the intercalation of 568^{th} Li switches the reaction to endothermic as the next intercalating Li moves away from the host as depicted in Fig. 6(d). The process of Li intercalation is strongly influenced by environmental factors, host material properties and guest-host interaction. The performance parameters of battery such as capacity, OCV and cycle life are determined by the lithiation energy due to which optimizing lithiation energy is essential for developing high-capacity anodes. Figure-6 demonstrates the computed valued of lithiation energy in LTO host. The detailed comparison of adsorption energy and storage capacity for 1.2 nm, 1.5 nm, 3.4 nm structures for pure LTO and 3.4 nm cluster C-Ti doped LTO structure is shown below in figure-7(a) and figure-7(b) respectively.

The doping of carbon in LTO appeared to increase the number of intercalating Li atoms in the host which points to improvement in storage capacity of LIBs. The defect engineering has been known to optimizes the charge transfer resistance and enhances the rate capability of anode materials [49].

3.4. Storage capacity of LTO

The calculation of storage capacity of a material is essential for its utilization as an electrode [50]. The storage capacity of transition metal oxides has been evaluated for application as anode material in LIBs on the basis of relevant chemical reactions for conversion. To determine a material's theoretical capacity equation-(2) is utilized [51]. The value of storage capacity of an anode material in LIBs is referred to the amount of charge stored in the electrode per unit mass and is usually represented in milliampere-hours per gram [52]. The Li concentration in LTO determines its storage capacity which is crucial for optimizing the electrochemical performance of the battery. The exceptional increase in the capacity to 1308mAh/g has been observed in porous nitrogen-doped carbon nanofibers by embedding red phosphorus nanoparticles of about 97.7 nm size using the electrospinning approach for sodium-ion batteries [53]. Similarly, the enhancement in lithium-ion storage in titanium dioxide nanoparticles have been reported in literature by utilizing the co-doping of carbon and sulfur. The doped TiO_2 nanoparticles displayed about 83 % capacity retention as compared to the undoped material [54]. The number of Li atoms stored in LTO nanoparticles as anode material for different sizes appeared as 42 atoms in 1.2 nm, 82 atoms in 1.5 nm, and 672 atoms in 3.4 nm. The respective computed values of the storage capacity are 379.46 $mAhg^{-1}$, 277.29 $mAhg^{-1}$ and 184 $mAhg^{-1}$ for 1.2 nm, 1.5 nm and 3.4 nm sized LTO as depicted in Fig. 8. The number of intercalated Li atoms increased in carbon doped structure resulting rise in storage capacity of the anode. The computed value for C_{Ti} based LTO is thus 1057 mAh/g as shown in Fig. 8(d) which is four times larger than that of the pristine material [55]. The structural changes upon carbon doping reduced the particle size which provides more active sites owing to an increased active surface area when compared with the undoped LTO [56].

The carbon doping in 3.4 nm cluster introduces the oxygen vacancies and Ti^{3+}/Ti^{2+} states which increases the number of active sites for the intercalation of additional Li-ions resulting the decrease in the energy barrier for Li-ion insertion which in return causes the increases in the storage capacity up to 1057 mAh/g. In addition to that the reduction of

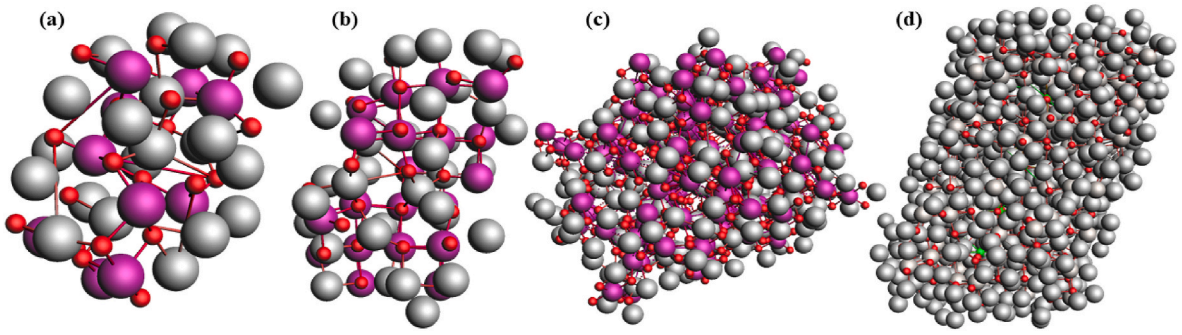

Figure-5. The optimized structure of LTO with (a) 13 Li atoms intercalation, (b) with 19 Li atoms intercalation (c) with 101 Li atoms interaction into carbon doped LTO (d) with 568 Li atoms.

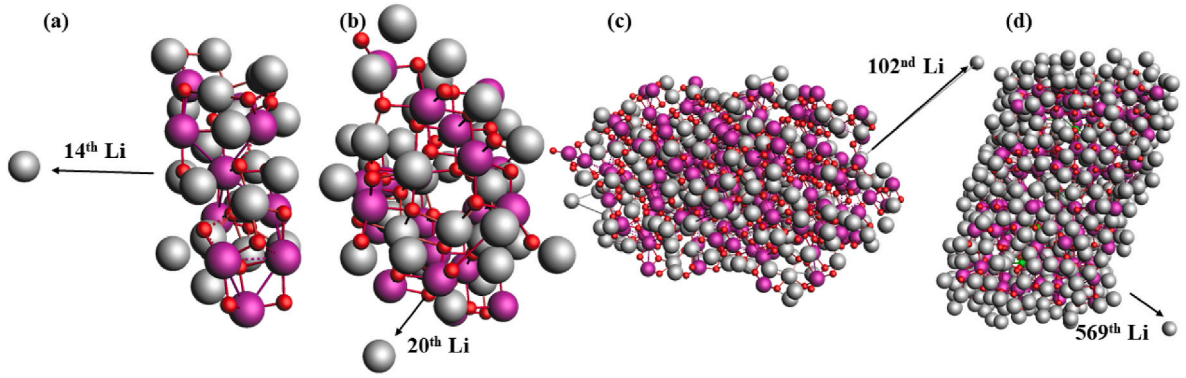

Figure-6. The optimized structure of LTO when further intercalating Li atom move away from the host (a) 14 Li atom intercalation (b) 20 Li atoms intercalation (c) 102 Li atoms intercalation and carbon doped LTO (d) 569 Li atoms.

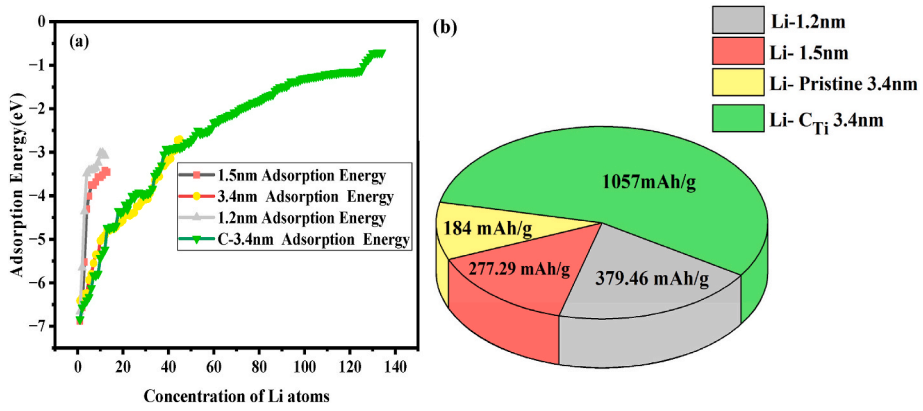

Figure-7. The computed values of (a) adsorption energy of Li atoms as a function of concentration and (b) Storage capacity of pure LTO and C- LTO.

material size to nanoscale plays a pivotal role in increasing the storage capacity enabling rapid kinetics by reducing the Li^+ diffusion distances even at high current densities. When the titanium atoms are replaced with smaller and more electronegative carbon atoms, the defects and vacancies are created within the structure which provides the additional space to store the lithium ions. In addition, the synergetic effects of doping and size reduction lowers the diffusion barrier by facilitating the faster and efficient charging/discharging cycles. This drastic improvement in the capacity of LTO anode makes it a potential candidate for next generation anodes for LIBs.

3.5. Open circuit voltage (OCV)

The OCV values demonstrates the energy per unit charge available for external circuit and provide the insights into electrochemical character of the battery and is calculated using equation-(3) [57,58]. The OCV is a critical parameter for assessing the performance anode in LIBs. The material's maximum storage capacity is considered only at the Li concentration, where there is either a positive voltage or absence of visible clustering [59]. As shown in fig-9, the increase in the Li concentration causes decrease in voltage values, thereby enhancing the battery performance. The average lithiation/delithiation voltage of Li for 1.2 nm LTO cluster in LIBs is calculated to be 3.08 V as shown in fig-8a. Meanwhile the 1.5 nm cluster reveals the higher average voltage span of 3.40 V depicted in fig-8b. Similarly, fig-8c represents the average voltage of 3.4 nm cluster for both pristine and C_{Ti}-doped LTO spans at 2.706 V and 0.708 V respectively. The significant lower voltage in carbon doped (0.708 V vs. Li^+/Li) structure represents its potential as a high-performance anode material due to high output voltage obtained.

3.6. Diffusion pathways

The migration paths of intercalated Li in the host LTO were studied using climbing image nudge simulations (Cl-NEB). This method offers a worthwhile analysis of energy dynamics, including critical points, energy amplification along the pathway, and energy reduction in alternative orientations. The energy barrier, inversely related to diffusion rate, is determined through NEB calculations, providing valuable insights into battery charging and discharging rates. The intercalating Li atoms while traversing the host material encounter an energy barrier which significantly influences the efficiency of battery charging. The modeling of different paths of Li in LTO is carried out through different pathways to explore the process of intercalation of each guest atom in the host structures. Two different pathways were considered for lithium migration into the host layers i.e. along x-axis and along y-axis. Fig. 10 (a) represents two different pathways for lithium atoms in 1.2 nm cluster showing the energy barriers of 0.86 eV for path 1 and 0.91 eV for path 2. The favorable migration pathways for 1.5 nm cluster, as depicted in Fig. 10 (b), depicts the energy barrier of 0.93 eV and 0.75 eV for path1 and path 2 respectively. As illustrated in figure-10(c) and 10(d) the diffusion barrier of Li atoms decreases after 5 % carbon doping representing the second favorable path with energy barrier of 0.69 eV and 0.46 eV respectively (see Fig. 11).

We consider the Li-ion adsorption rate in the calculation, as Li-ion migration energy barrier depending on Li concentration [14,67-69]. In this regard, we examined two limiting cases here, namely migration of a dilute Li ion and migration of a dilute Li vacancy. On the other hand, in case of dilute Li ion, one Li ion is adsorbed on a supercell of LTO while for the dilute Li vacancy case, one Li ion is removed from the supercell of the fully saturated structure to generate the vacancy [70].

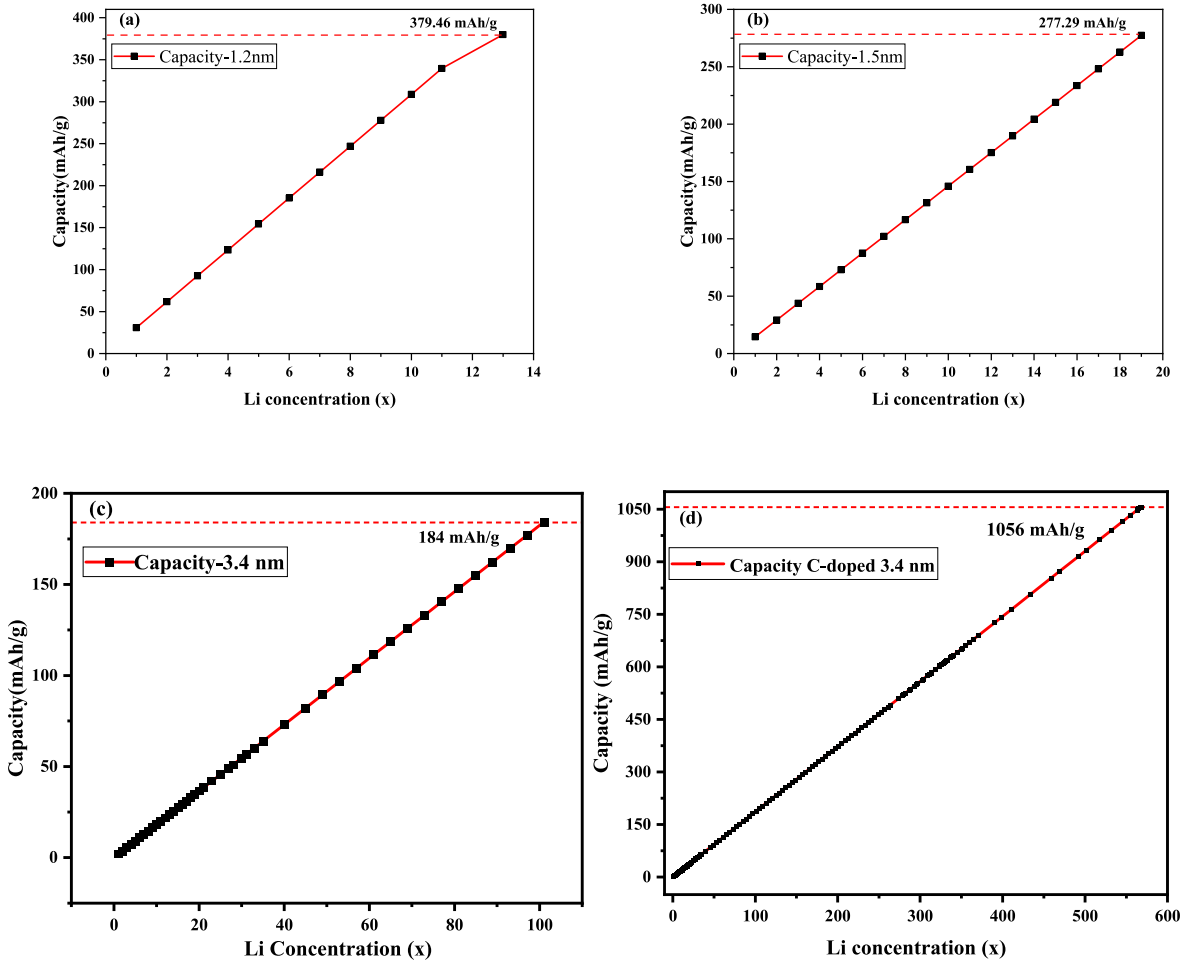

Figure-8. The calculated storage capacity of LTO as an anode for use in LIBs for (a) 1.2 nm(b) 1.5 nm and (c) 3.4 nm and (d) C-doped 3.4 nm.

The calculated energy barrier in the direction of vacancy migration was found to be 1.4 eV, 0.5 eV, 1.75 eV and 1.5 eV for 1.2 nm, 1.5 nm, 3.4 nm and C-doped 3.4 nm respectively. The energy barrier obtained in case of fully loaded structure with vacancy-dilute situation is more than that of the dilute-Li structure [71].The enhanced vacancy mobility in smaller nanoparticle cluster of 1.5 nm LTO system is observed with lowest energy barrier of 0.5 eV which can result due to increased structural flexibility and reduction of steric hindrance in nanoscale as compared to the larger cluster with energy barrier of 1.75 eV for 3.4 nm cluster. The higher energy barrier of 1.4 eV in 1.2 nm cluster may result due to the surface reconstructions or edge effects which tends to trap the vacancies temporarily. Furthermore, the vacancy migration barrier in the carbon doped cluster reduced from 1.75 eV to 1.5 eV which clearly indicates that the C-doping facilitates the vacancy diffusion. This improvement in the diffusion barrier arises due to the electronic structure modifications introduced due to replacement of titanium with carbon atoms. In addition to that, preferential migration pathways may be created due to the strain fields introduced due to the carbon doping. From a practical perspective, the reduction in the energy barrier of C-doped LTO at 1.5 eV indicates faster Li^+ diffusion kinetics and superior cyclic stability.

3.7. Diffusion Co-efficient and ionic conductivity

The diffusion coefficient plays a pivotal role in inspecting the efficacy of anode material. The MD simulations were performed in temperature range of 300 K–900 K to investigate the diffusion coefficient. The temperature-dependent behavior of diffusivity strengthens our understanding of the transport properties. The fact that the ionic conductance (σ) is influenced by the variations in the host structure caused by the guest atom which can be determined using equation (8). Mean square displacement (MSD) for intercalating Li atoms is determined using equation-(6). The trajectory analysis points that diffusion occurs more rapidly at elevated temperatures, which is attributed to faster charging [72]. The diffusion rates of Li atoms in the host materials are comparable to those reported for anode materials used in LIBs [73-76]. Regardless of the advancement in anode materials [77-79], there is the need of further improvement to keep up with the consumer demands of high energy density, faster charging and improved stability. In case of graphite which dominates the commercial market, the low storage capacity motivates research into doping of LTO to enhance the electrochemical characteristics. The MD simulations indicate the diffusion coefficient as $4.3x10^{-12}$ m^2/s, $5.0x10^{-12}$ m^2/s, $0.83x10^{-12}$ m^2/s and $1.72\ x10^{-8}$ m^2/s for 1.2 nm, 1.5 nm, 3.4 nm and doped 3.4 nm respectively. The carbon doped structure exhibits the excellent diffusion coefficient of $1.72x10^{-8}$ m^2/s indicating up to 4 orders of higher magnitude then other undoped structures shown in Fig. 12. This causes due to the low energy barriers for Li-ion diffusion as carbon dopants introduce the additional charge carriers which enhance the ionic conductivity of structure.

The ionic conductivity is another crucial parameter to access the anodic capability of a material as it determines how fast Li can travel in the host structure. Fig. 13(a), (b), (c) and (d) show the calculated ionic conductivity of LIBs which appeared as $5.32\ x\ 10^{-3}$ Sm^{-1}, $0.19\ x\ 10^{-2}$ Sm^{-1},$9.32\ x\ 10^{-2}$ Sm^{-1} and $7.33\ x\ 10^{-3}$ Sm^{-1} for 1.2 nm, 1.4 nm, 3.4 nm and C-3.4 nm respectively. The findings point to ease of Li to

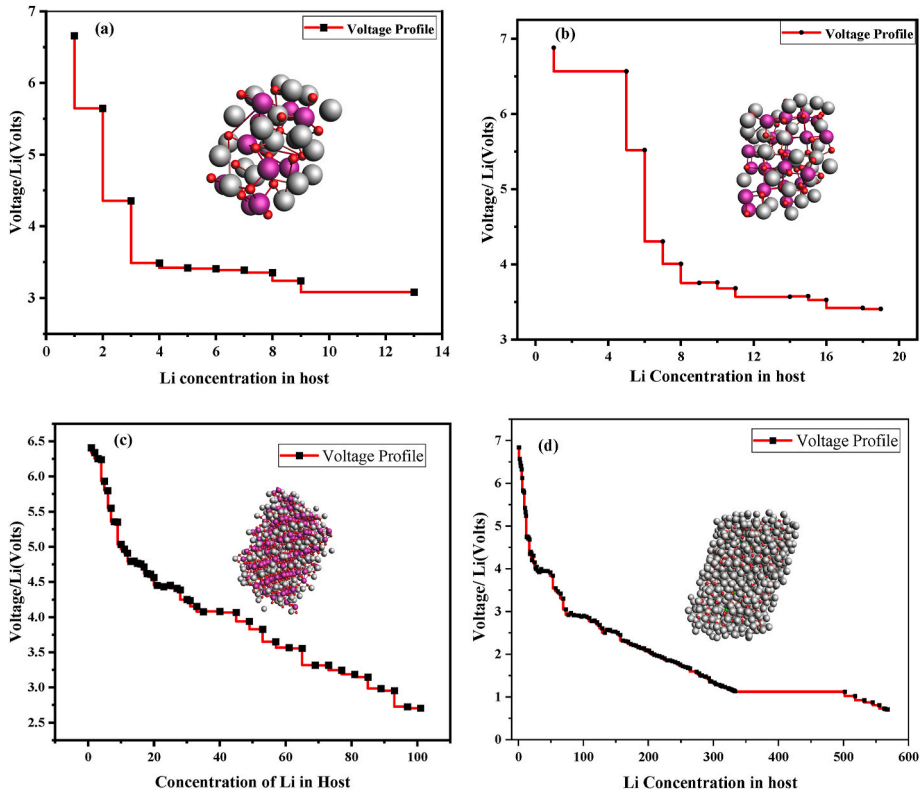

Figure-9. The calculated open circuit voltage of LTO as an anode for LIB for (a) 1.2 nm, (b) 1.5 nm, (c) 3.4 nm and (d) C-doped 3.4 nm.

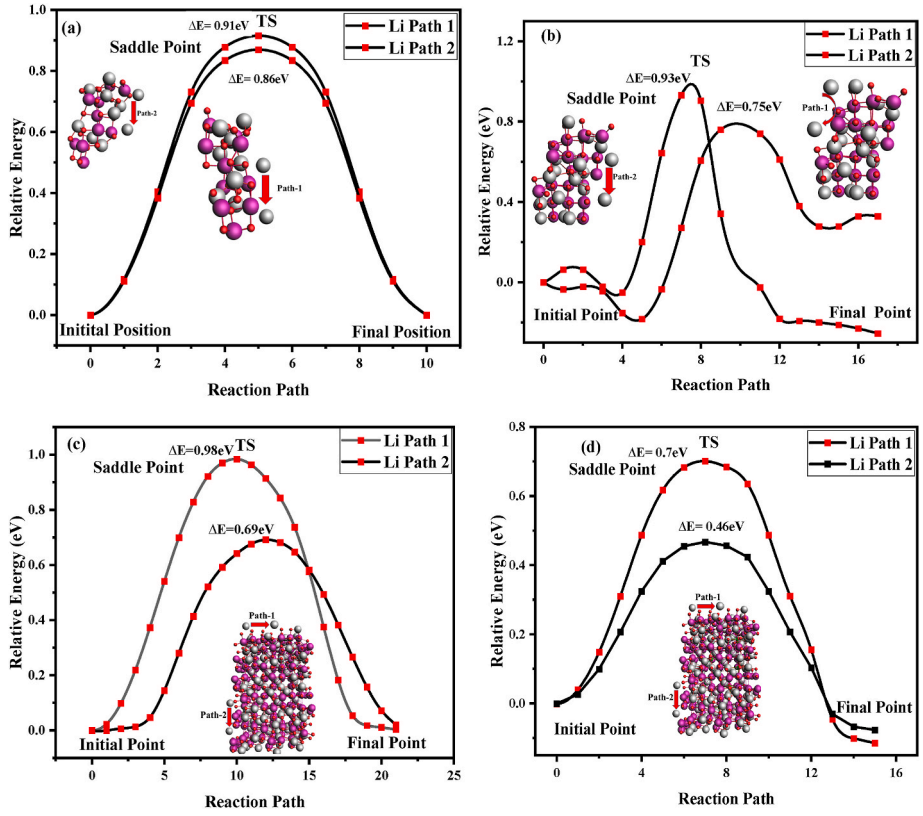

Figure-10. Diffusion Energy pathways of Li in LTO nanoparticles for (a) 1.2 nm (b) 1.5 nm (c) 3.4 nm pristine LTO and (d) 3.4 nm C_{Ti} doped LTO.

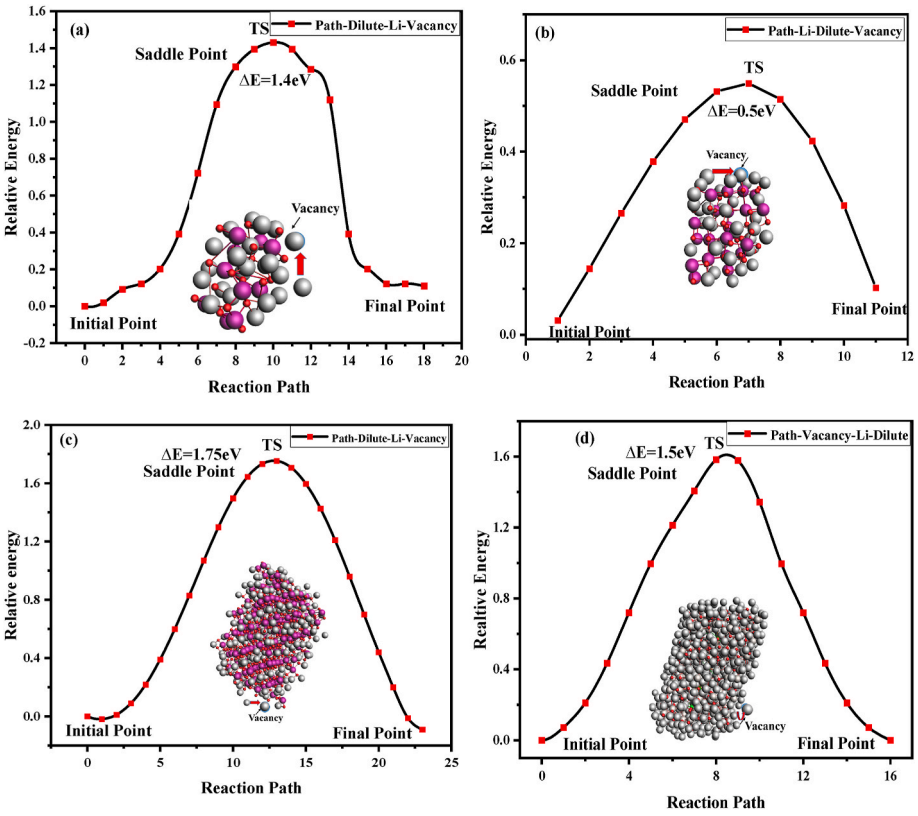

Figure-11. Diffusion energy vacancy migration pathways for Li in LTO for (a) 1.2 nm (b) 1.5 nm (c) 3.4 nm pristine LTO and (d) 3.4 nm C_{Ti} LTO. The barrier values are calculated for dilute -metal host structure and dilute lithium vacancy fully loaded host structure.

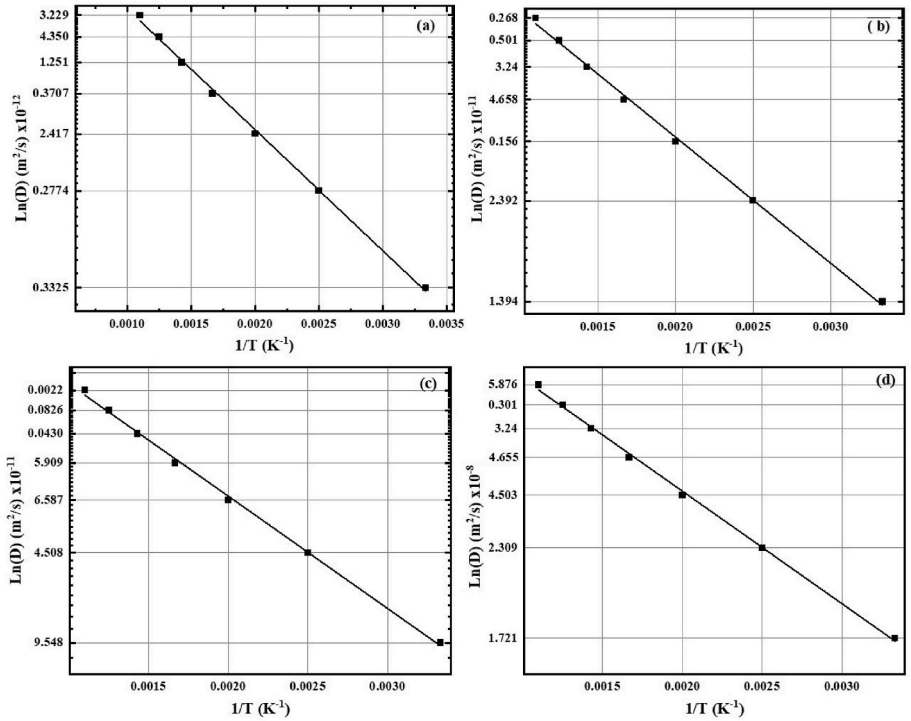

Figure-12. Diffusion co-efficient of LTO after the intercalation of Li atoms in (a) 1.2 nm (b) 1.5 nm, (c) 3.4 nm and C-doped 3.4 nm.

intercalate and de-intercalate in the host matrix of LTO.

The ionic conductivity in 1.4 nm cluster was lowest due to extreme surface disorders and incomplete ionic pathways at ultra-small dimensions. In contrast, the higher ionic conductivity in 1.2 nm cluster indicates that it is the optimal particle size for balance ionic transport and structural stability. These findings align with the previous studies on

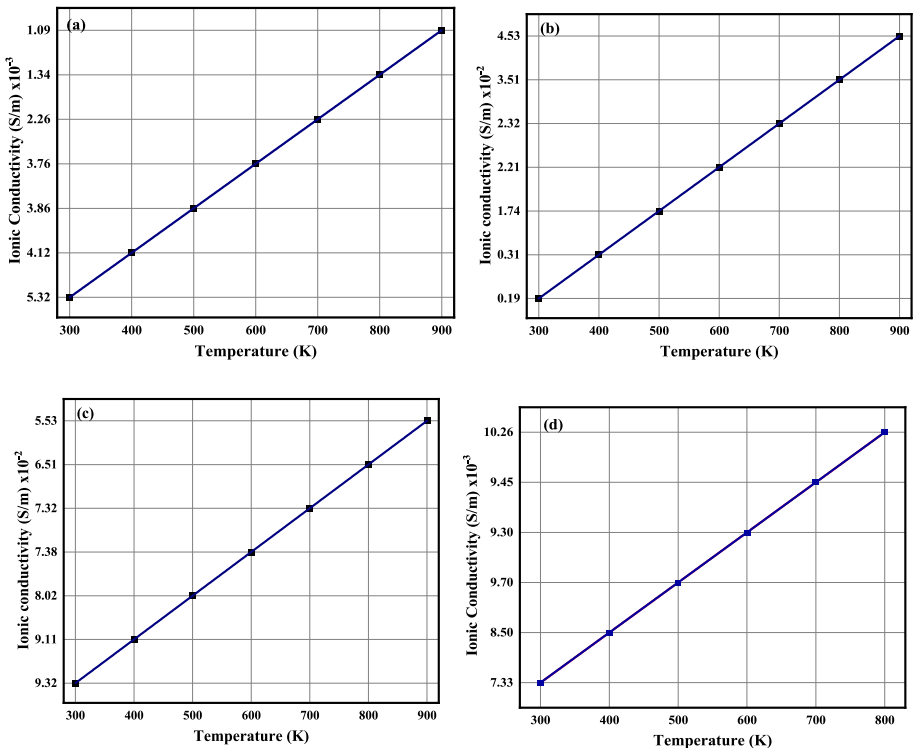

Figure-13. The ionic conductivity of LTO (a) 1.2 nm after Li adsorption (b) 1.4 nm after Li adsorption (c) 3.4 nm after Li adsorption (d) C- 3.4 nm after Li adsorption.

the nanostructured anodes in which the mid-range particle size often contains better conductivity. These finding indicates the importance of synergetic effects of size control and doping for optimizing the high-performance anode materials for LIBs.

A common misconception rises when dealing with nanoscale materials: on considering the fact that diffusivity and conductivity are intrinsic bulk properties of a material, they can exhibit substantial size dependence at the nanoscale. The reported literature categorically demonstrates that central mechanism of ion migration remains inherent to the material's properties, the ionic conductivity diffusivity in nanomaterials depend on several factors including particle size, defect concentrations and distribution, surface area, grain boundaries, which are characteristic features at nanoscale[85–87].

3.8. Hirshfield charge analysis

Hirshfeld charge analysis is a resourceful method for examining intermolecular interactions in solids [80]. The contour surfaces and colour-coded fingerprint plots and are utilized to visualize these interactions; a spectrum ranging from red (shorter) to white and blue (longer) indicates distances that are shorter or longer than the sum of the van der Waals (vdW) radii. In order to comprehend the electrochemical mechanism at play, Hirshfeld charge analysis is performed to investigate the host's charge distribution before and after intercalation. The intermolecular interaction and behavior of electrode during charging and discharging cycles in energy storage devices is to determine the electrode's ability to accumulate and release charge with associated energy loses. Figure-14 depicts all the major and minor charges in the structure.

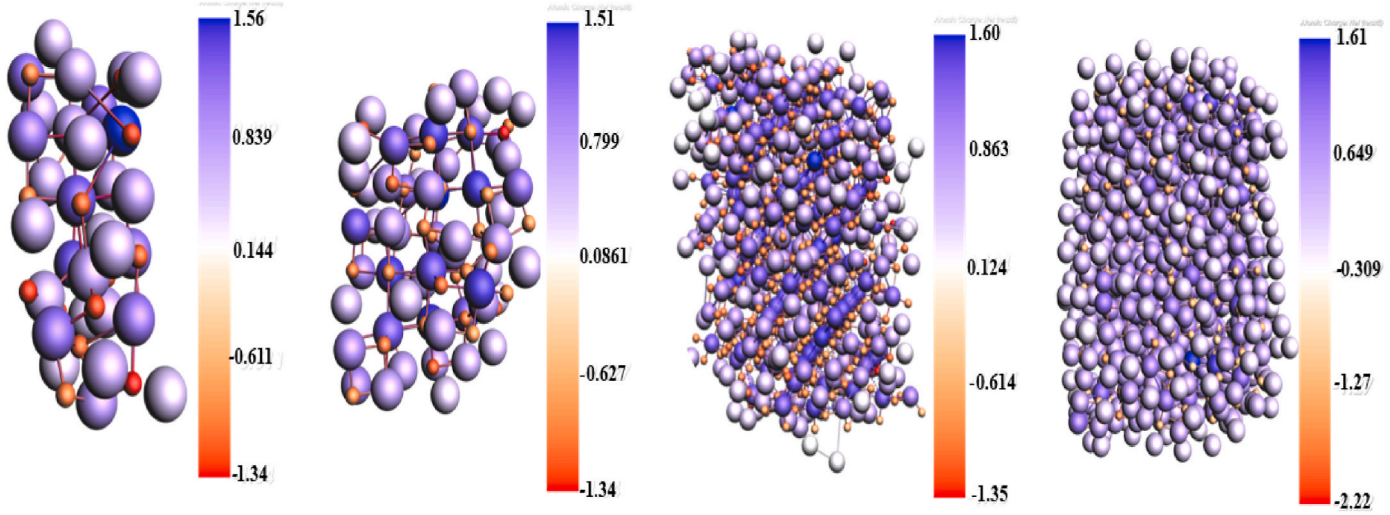

Figure-14. The Hirshfeld charge analysis of LTO with (a) Li intercalation in 1.2 nm (snapshot along the x-axis), (b) Li intercalation in 1.5 nm (snapshot along the x-axis), (c) Li intercalation in pristine 3.4 nm (snapshot along the x-axis) and (d) Li intercalation in C_{Ti} 3.4 nm.

Li bears a positive charge after intercalation in the host structure which represents that charge is transferred from li to the host LTO structure.

3.9. Current voltage (I–V) characteristics

To model the electron transport in solid electrolyte interface (SEI), the NEGF calculations of pure LTO and Li adsorbed structures were conducted as shown in fig-15. The voltage provided to the host material using two leads of gold in the circuit. Since we are interested in the electron flow caused by positive voltages, the IV-curves are calculated within the −5 to +5 V range. Fig. 15(a), (b), 15(c) and 15(d) show Pure LTO (1.2 nm), Li-adsorbed LTO (1.2 nm), pure LTO (1.4 nm) and Li-adsorbed LTO respectively. Fig. 14 (e, f) shows that pure LTO has a minimum current of 0.09 μA (1.2 nm), 0.13 μA (1.4 nm), which significantly increases to 59 μA and 184 μA, when Li atoms are intercalated in the host material.

In addition, ethylene carbonate (EC) was used near the LTO anode material to explore electron transport, as depicted in Fig. 16(a) for pure (1.2 nm), 16(b) for Li, 16(c) for pure LTO (1.4 nm), and 16(d) for Li (1.4 nm). The IV-curves in Fig. 16(e) and (f) indicates that, (i) a large rise in current upon intercalation, and (ii) a prominent drop in current after addition of the electrolyte. The study of the intercalated host's IV-curves suggests that the current decrease is caused by electron transfer processes. The first process indicates the electron donation which leads to the formation of SEI on surface of the anode [81]. The SEI forms during the battery manufacturing process's activation step. Metal ions may readily pass across the layered structure of the battery stack, which comprises both SEI layers [82]. When the current (I) is supplied to the battery, the electrochemical reactions take place at the negative electrode, as follows:

$$I_{ch} = I_{ch}^{tr} + I_{SEI} \tag{9}$$

The current (I_{ch}^{tr}) refers to the charge transfers as it facilitates intercalation of the metal ions in negative electrodes, while I_{SEI} is the current associated with SEI creation processes. The principal electrochemical storage process requires the majority of the current to function [83]. SEI components cause a significant reduction in current (measured by ΔI_X) in comparison to the case without an electrolyte. It appears that valance state of intercalating Li atoms affects the concurrent shift of electrons from EC and Li ions to create SEI. The additional electrons in a multivalent ion battery can speed up the production of stable SEI, which is crucial for devolving the cost-effective and efficient metal ion batteries [84].

4. Conclusion

The anodic properties of lithium titanate oxide ($Li_4Ti_5O_{12}$) nanoparticles are studied to investigate the structural, thermal and electrochemical properties associated with variation of size, and carbon doping. AIMD studies confirm thermal stability of the host material, while Cl-NEB computations indicate that energy barriers for lithium and vacancy diffusion are small where the lowest barrier is found in the carbon doped structure at 0.45 eV. This is particularly true at the carbon site for 3.4 nm which when introduced at the titanium site, the storage capacity is increased to 1057 $mAhg^{-1}$. The material is also confirmed to be able to keep safe and efficient with OCV of 3.08 V, 3.40 V, 2.70 V, and 0.70 V for 1.2 nm, 1.5 nm, 3.4 nm, and carbon doped $Li_4Ti_5O_{12}$ structure, respectively. The diffusion coefficient analysis at 300 K and 900 K has demonstrated a very good rate performance of the C doped 3.4 nm structure (1.72×10^{-8} m^2/s) and is extremely beneficial in LIB applications. This study demonstrates a significant size dependence of diffusivity and conductivity, in contrast to the fact that these parameters are intrinsic material properties at bulk, indicating a complex relationship of surface effects and quantum phenomena. The theoretical predictions made in this work offer helpful insights into the atomic-level mechanisms on LTO to improve performance using carbon doping, it is crucial to mention that the experimental realization will encounter significant experimental challenges.

CRediT authorship contribution statement

Abdul Majid: Writing – review & editing, Supervision, Methodology, Conceptualization. **Fiza Shafique:** Writing – original draft, Methodology, Investigation, Data curation. **Sawaira Tasawar:** Methodology, Investigation, Data curation. **Mohammad Alkhedher:** Visualization, Validation, Methodology. **Salah Ud-Din Khan:** Visualization, Validation, Methodology. **Kamran Alam:** Visualization, Validation, Methodology, Investigation. **Sajjad Haider:** Visualization, Validation, Methodology, Investigation.

Ethics statement

The authors have nothing to report.

Declaration of competing interest

The authors declare that they have no known competing financial

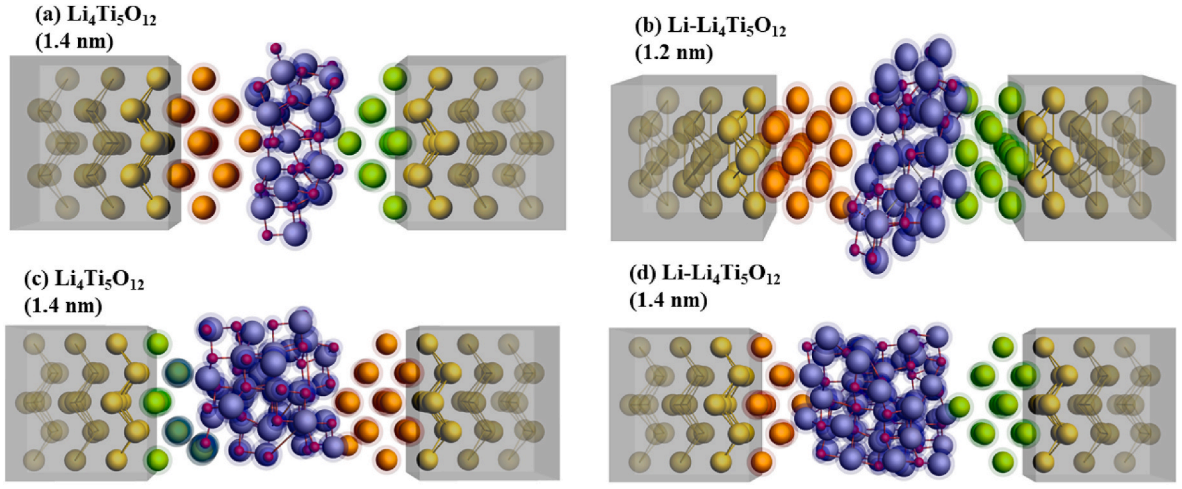

Fig. 15. The view of NEGF setup of (a) pure LTO (1.2 nm), (b) Li adsorbed LTO (1.2 nm), (c) pure LTO (1.4 nm) and (d) Li adsorbed LTO (1.4 nm). The proposed anode material is placed between gold lead. (For interpretation of the references to colour in this figure legend, the reader is referred to the Web version of this article.)

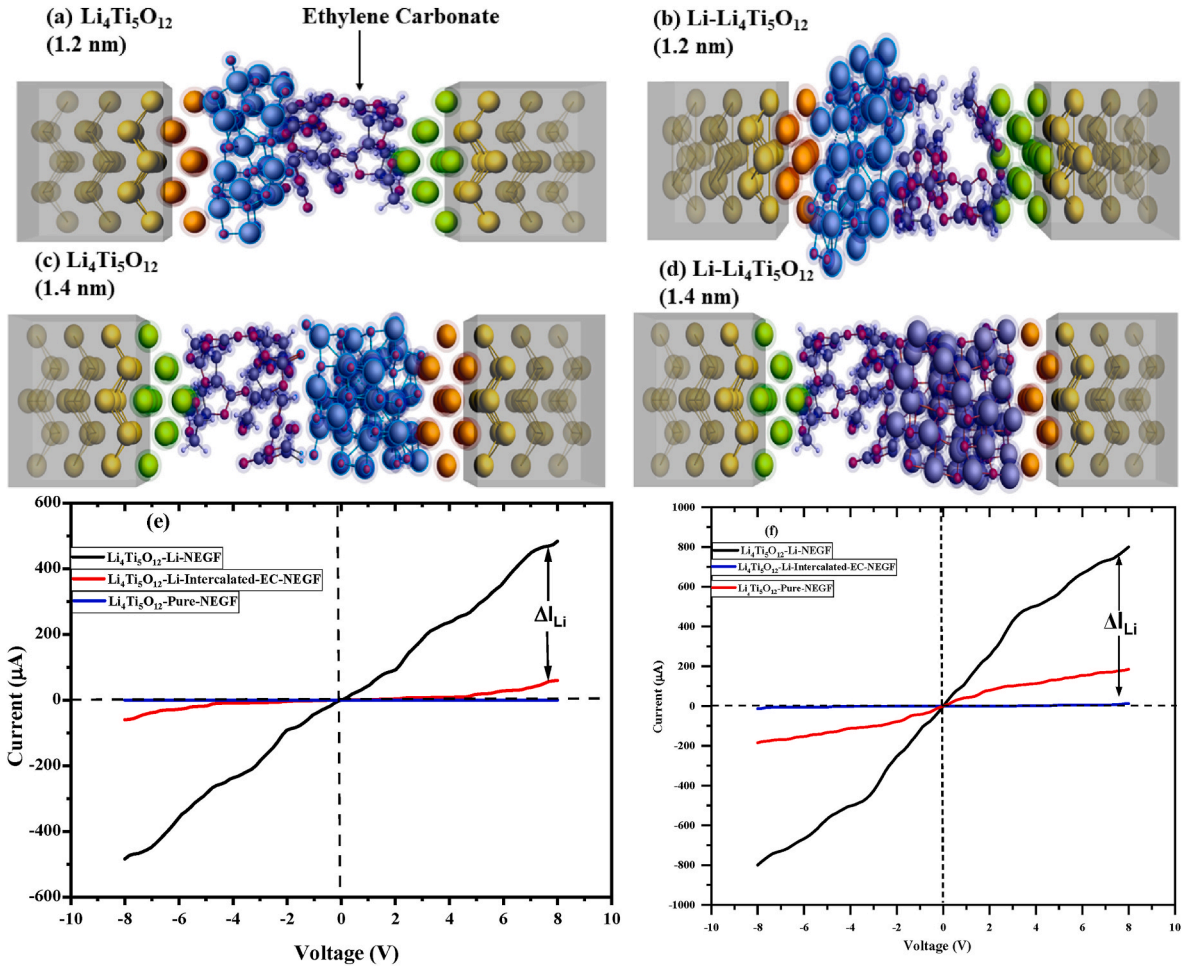

Fig. 16. NEGF setup illustrating the deposition of ethylene carbonate (EC) electrolyte between gold lead and battery anode in the form of (a) pure LTO (1.2 nm) (b) Li adsorbed LTO (1.2 nm) (c) pure LTO (1.4 nm) (d) Li adsorbed LTO (1.4 nm). The Current-Voltage (IV) characteristics illustrating the comparison of IV curves of (e) pure LTO (1.2 nm), Li intercalated LTO and EC plus Li adsorbed LTO, (f) pure LTO (1.4 nm), Li intercalated LTO, and EC plus Li adsorbed LTO. Here, the change in current with and without EC is demonstrated above. (For interpretation of the references to colour in this figure legend, the reader is referred to the Web version of this article.)

interests or personal relationships that could have appeared to influence the work reported in this paper.

Acknowledgments

The authors sincerely appreciate funding from Ongoing Research Funding Program (ORF-2025-399), King Saud University, Riyadh, Saudi Arabia.

Data availability

Data will be made available on request.

References

[1] M.I. Hoffert, et al., Advanced technology paths to global climate stability: energy for a greenhouse planet, science 298 (5595) (2002) 981–987.
[2] A. Midilli, I. Dincer, M. Ay, Green energy strategies for sustainable development, Energy Policy 34 (18) (2006) 3623–3633.
[3] C. Bussar, et al., Large-scale integration of renewable energies and impact on storage demand in a European renewable power system of 2050—sensitivity study, J. Energy Storage 6 (2016) 1–10.
[4] Z. Zhu, et al., Rechargeable batteries for grid scale energy storage, Chem. Rev. 122 (22) (2022) 16610–16751.
[5] D. Languino, An Exploratory Study on the End-Of-Life Batteries Supply Chain: the Automotive Sector Perspective, 2023. Politecnico di Torino.
[6] A. Perner, J. Vetter, Lithium-ion batteries for hybrid electric vehicles and battery electric vehicles, in: Advances in Battery Technologies for Electric Vehicles, Elsevier, 2015, pp. 173–190.
[7] J. Peng, G. Ji, X. Wang, Cycling performance and failure behavior of lithium-ion battery Silicon-Carbon composite electrode, J. Electroanal. Chem. 956 (2024) 118095.
[8] L. Zhao, D. Dvorak, M. Obrovac, Layered amorphous silicon as negative electrodes in lithium-ion batteries, J. Power Sources 332 (2016) 290–298.
[9] M.T. McDowell, et al., 25th anniversary article: understanding the lithiation of silicon and other alloying anodes for lithium-ion batteries, Adv. Mater. 25 (36) (2013) 4966–4985.
[10] C. Peng, et al., A chronicle of titanium niobium oxide materials for high-performance lithium-ion batteries: from laboratory to industry, Carbon Neutralization 3 (6) (2024) 1036–1091.
[11] Y.S. Shakespeare, Transition Metal Oxide Composite Nanomaterials as Anodes in Lithium-Ion Energy Storage Devices, UCL (University College London), 2022.
[12] Y.S. Worku, et al., Recent advancements of niobium and tantalum-based materials: from design engineering to energy storage applications, ChemistrySelect 10 (3) (2025) e202405649.
[13] J. Zheng, et al., Advanced anode materials of potassium ion batteries: from zero dimension to three dimensions, Nano-Micro Lett. 13 (2021) 1–37.
[14] A. Majid, et al., Uncovering the Potential of Two-Dimensional SrRuO 3 as anode material in Li, Na, Mg, Ca, K, and Zn ion Batteries: first-Principles investigations of structural, electronic and electrochemical properties, J. Energy Storage 105 (2025) 114634.
[15] A. Majid, et al., On the prospects of using B4C3 as a potential electrode material for lithium-ion batteries, Mater. Sci. Semicond. Process. 176 (2024) 108320.
[16] A. Majid, et al., Advancing the technology of lithium, magnesium, and aluminum-ion batteries via Chromium Ditelluride as a novel anode material, Battery Energy 4 (1) (2025) 20240027.

[17] H. Song, et al., An upper limit of Cr-doping level to Retain zero-strain characteristics of Li4Ti5O12 anode material for Li-ion batteries, Sci. Rep. 7 (1) (2017) 43335.
[18] J. Shu, Electrochemical behavior and stability of Li 4 Ti 5 O 12 in a broad voltage window, J. Solid State Electrochem. 13 (2009) 1535–1539.
[19] H. Yan, et al., A review of spinel lithium titanate (Li4Ti5O12) as electrode material for advanced energy storage devices, Ceram. Int. 47 (5) (2021) 5870–5895.
[20] Z. Tong, et al., Multivalent-ion Electrochromic energy Saving and storage devices, Adv. Funct. Mater. (2024) 2308989.
[21] N. Takami, et al., High-power and long-life lithium-ion batteries using lithium titanium oxide anode for automotive and stationary power applications, J. Power Sources 244 (2013) 469–475.
[22] Z. Zhang, et al., Hydrothermal synthesis of Li4Ti5O12 microsphere with high capacity as anode material for lithium ion batteries, Ceram. Int. 39 (3) (2013) 2695–2698.
[23] B. Dandigunta, et al., α-Graphyne with ultra-low diffusion barriers as a promising sodium-ion battery anode and a computational scheme for accurate estimation of theoretical specific capacity, Nanoscale 16 (36) (2024) 16900–16912.
[24] H. Khattab, et al., P6C5 monolayer as promising anode for high-performance sodium-ion batteries: insights from DFT and AIMD study, J. Power Sources 614 (2024) 235000.
[25] P. Kandwal, Harnessing two dimensional B2C monolayer as an anode material in potassium ion batteries: DFT and AIMD study, Comput. Mater. Sci. 246 (2025) 113435.
[26] M. Fardi, et al., DFT and AIMD evaluation of boron-doped Biphenylene as an anode material in lithium-and sodium-ion batteries, Adv. Mater. Interfac. 11 (35) (2024) 2400522.
[27] T. Ahmed, A.A. Piya, S.U.D. Shamim, Recent advances in Zr and Hf-based MXenes and their hetero-structure as novel anode materials for Ca-ion batteries: theoretical insights from DFT approach, Nanoscale Adv. (2024).
[28] P. Patel, et al., Two-dimensional α-SiX (X= N, P) monolayers as efficient anode material for Li-ion batteries: a first-principles study, ACS Appl. Nano Mater. 6 (3) (2023) 2103–2115.
[29] K. Tao, et al., Nitrogen and sulfur co-doped carbon-coated Li4Ti5O12 composite to enhance lithium storage properties, Ionics 30 (4) (2024) 2083–2091.
[30] T. Meng, et al., Chitosan-confined synthesis of N-doped and carbon-coated Li4Ti5O12 nanoparticles with enhanced lithium storage for lithium-ion batteries, J. Electrochem. Soc. 165 (5) (2018) A1046.
[31] M. Widmaier, et al., Influence of carbon distribution on the electrochemical performance and stability of lithium titanate based energy storage devices, Electrochim. Acta 247 (2017) 1006–1018.
[32] X. Jiang, et al., Synthesis of dual-modified Fe-doped and carbon-coated Li4Ti5O12 anode based on industrial H2TiO3 for Li-ion batteries, Sci. Rep. 13 (1) (2023) 15118.
[33] K.X. Wang, X.H. Li, J.S. Chen, Surface and interface engineering of electrode materials for lithium-ion batteries, Adv. Mater. 27 (3) (2015) 527–545.
[34] L. Yu, et al., Recent developments of nanomaterials and nanostructures for high-rate lithium ion batteries, ChemSusChem 13 (20) (2020) 5361–5407.
[35] H.-R. Yao, Y.-X. Yin, Y.-G. Guo, Size effects in lithium ion batteries, Chin. Phys. B 25 (1) (2015) 018203.
[36] M. Apostolopoulou, D. Vernardou, S. Passerini, Optimization strategies of hybrid lithium titanate oxide/carbon anodes for lithium-ion batteries, Nanomaterials 14 (22) (2024) 1799.
[37] H. Zhang, et al., Li4Ti5O12 spinel anode: Fundamentals and advances in rechargeable batteries, InfoMat 4 (4) (2022) e12228.
[38] J.Z. Lu Zhang, Benjun Xu, Enhancing the Electrochemical performance of Li4Ti5O12 anode materials by codoping with Na and Br, J. alloys. compounds 903 (163962) (2022).
[39] Y.X. Ting-Feng Yi, Yan-Rong Zhu, Rong- Sun Zhu, Haoyu Shen, Structural and thermodynamic stability of Li4Ti5O12 anode material for lithium-ion battery, Journel of power sources 222 (2013) 448–454.
[40] G.L. Hart, R.W. Forcade, Generating derivative structures from multilattices: Algorithm and application to hcp alloys, Phys. Rev. B Condens. Matter 80 (1) (2009) 014120.
[41] G. Bergerhoff, et al., The inorganic crystal structure data base, J. Chem. Inf. Comput. Sci. 23 (2) (1983) 66–69.
[42] M. Dalton, et al., Structure of the Li1+ xTi2− xO4 superconducting system: a neutron diffraction study, Phys. C Supercond. 221 (1–2) (1994) 149–156.
[43] P. Bhauriyal, A. Mahata, B. Pathak, Graphene-like carbon–nitride monolayer: a potential anode material for Na-and K-ion batteries, J. Phys. Chem. C 122 (5) (2018) 2481–2489.
[44] J.P. Naeyaert Pieree, C.D.L. Maxim Avdeev, Synthesis, electrochemistry and transition metal-doping of monoclinic $Li_4Ti_5O_{12}$ and $Na_4Ti_5O_{12}$, Solid State Ionics 353 (2020) 115375.
[45] Y. Liu, J. Lian, Z. Sun, M. Zhao, Y. Shi, H. Song, The first-principles study for the novel optical properties of LiTi2O4, Li4Ti5O12, Li2Ti2O4 and Li7Ti5O12, Chem. Phys. Lett. 677 (2017) 114–119.
[46] A. Jabeen, et al., Impacts of structural downscaling of inorganic molecular crystals-A DFT study of Sb2O3, Mater. Sci. Semicond. Process. 166 (2023) 107729.
[47] D. Andersson, B.W. Beeler, Ab initio molecular dynamics (AIMD) simulations of NaCl, UCl3 and NaCl-UCl3 molten salts, J. Nucl. Mater. 568 (2022) 153836.
[48] F. Holtstiege, et al., Pre-lithiation strategies for rechargeable energy storage technologies: Concepts, promises and challenges, Batteries 4 (1) (2018) 4.
[49] K.T. Nam, et al., Virus-enabled synthesis and assembly of nanowires for lithium ion battery electrodes, science 312 (5775) (2006) 885–888.
[50] S. Klein, et al., On the beneficial impact of Li2CO3 as electrolyte additive in NCM523‖ graphite lithium ion cells under high-voltage conditions, Adv. Energy Mater. 11 (10) (2021) 2003756.
[51] C. Zhang, et al., Transition metals doped borophene-graphene heterostructure for robust polysulfide anchoring: a first principle study, Appl. Surf. Sci. 534 (2020) 147575.
[52] J. He, J. Meng, Y. Huang, Challenges and recent progress in fast-charging lithium-ion battery materials, J. Power Sources 570 (2023) 232965.
[53] Y. Liu, et al., Red phosphorus nanoparticles embedded in porous N-doped carbon nanofibers as high-performance anode for sodium-ion batteries, Energy Storage Mater. 9 (2017) 170–178.
[54] S. Ivanov, et al., Enhanced lithium ion storage in TiO2 nanoparticles, induced by sulphur and carbon co-doping, J. Power Sources 326 (2016) 270–278.
[55] D. Datta, J. Li, N. Koratkar, V.B. Shenoy, Enhanced lithiation in defective graphene, Carbon 80 (2014) 305–310.
[56] L.T. Anh, et al., Improving the electrochemical performance of anatase titanium dioxide by vanadium doping as an anode material for lithium-ion batteries, J. Power Sources 243 (2013) 891–898.
[57] A. Sengupta, Lithium and sodium adsorption properties of two-dimensional aluminum nitride, Appl. Surf. Sci. 451 (2018) 141–147.
[58] C. Xiao, et al., Graphene-like BSi as a promising anode material for Li-and Mg-ion batteries: a first principle study, Appl. Surf. Sci. 563 (2021) 150278.
[59] N. Yadav, B. Chakraborty, T. Dhilip Kumar, First-principles design and investigation of siligraphene as a potential anode material for na-ion batteries, J. Phys. Chem. C 124 (21) (2020) 11293–11300.
[60] H. Wang, et al., Two-dimensional layered green phosphorus as an anode material for Li-ion batteries, ACS Appl. Energy Mater. 5 (2) (2022) 2184–2191.
[61] S. Yi, et al., Double-layer honeycomb AlP: a promising anode material for Li-, Na-, and K-ion batteries, J. Phys. Chem. C 124 (5) (2020) 2978–2986.
[62] S. Ma, et al., A novel two-dimensional whorled TiB4 as a high-performance anode material for Li-ion and Na-ion batteries, Appl. Surf. Sci. 639 (2023) 158083.
[63] C. Zhang, et al., Two-dimensional GeP 3 as a high capacity electrode material for Li-ion batteries, Phys. Chem. Chem. Phys. 19 (38) (2017) 25886–25890.
[64] B. Ball, C. Chakravarty, P. Sarkar, Two-dimensional covalent triazine framework as a promising anode material for Li-ion batteries, J. Phys. Chem. C 123 (50) (2019) 30155–30164.
[65] J. Park, S.A. Fatima, A DFT study of TiC3 as anode material for Li-ion batteries, Appl. Surf. Sci. 638 (2023) 158024.
[66] J. Rehman, et al., Highly conductive and stable two-dimensional WC4 acting as an efficient anode material for Alkali-metal ion batteries: Insight from DFT, J. Phys. Chem. C 127 (49) (2023) 23592–23600.
[67] X. Li, et al., Perovskite-type SrVO3 as high-performance anode materials for lithium-ion batteries, Adv. Mater. 34 (46) (2022) 2107262.
[68] H. Li, et al., Scalable production of few-layer boron sheets by liquid-phase exfoliation and their superior supercapacitive performance, ACS Nano 12 (2) (2018) 1262–1272.
[69] G.T.H. Nguyen, D.T. Nguyen, S.W. Song, Unveiling the roles of formation process in improving cycling performance of magnesium Stannide composite anode for magnesium-ion batteries, Adv. Mater. Interfac. 5 (22) (2018) 1801039.
[70] Z. Yao, et al., Discovery of calcium-metal alloy anodes for reversible Ca-ion batteries, Adv. Energy Mater. 9 (9) (2019) 1802994.
[71] J. Rehman, et al., Lithiation and sodiation of hydrogenated silicene: a density functional theory investigation, ChemSusChem 14 (24) (2021) 5460–5469.
[72] R. Trivedi, D. Bandyopadhyay, Study of adsorption and dissociation pathway of H2 molecule on MgnRh (n= 1–10) clusters: a first principle investigation, Int. J. Hydrogen Energy 41 (44) (2016) 20113–20121.
[73] X. Yang, et al., Tuning mixed electronic/ionic conductivity of 2D CdPS3 nanosheets as an anode material by synergistic intercalation and vacancy engineering, Adv. Funct. Mater. 32 (18) (2022) 2112169.
[74] M. Dynarowska, et al., Ionic conductivity and structural properties of Na2Ti3O7 anode material, Solid State Ionics 301 (2017) 35–42.
[75] J. Niu, Z. Zhang, D. Aurbach, Alloy anode materials for rechargeable Mg ion batteries, Adv. Energy Mater. 10 (23) (2020) 2000697.
[76] Y. Xu, et al., Vanadium oxide pillared by interlayer Mg2+ ions and water as ultralong-life cathodes for magnesium-ion batteries, Chem 5 (5) (2019) 1194–1209.
[77] Y. Zhao, et al., Recent developments and understanding of novel mixed transition-metal oxides as anodes in lithium ion batteries, Adv. Energy Mater. 6 (8) (2016) 1502175.
[78] G. Li, et al., Recent advances and perspectives of microsized alloying-type porous anode materials in high-performance Li-and Na-ion batteries, Energy Mater 2 (2022) 200020.
[79] L. Shi, T. Zhao, Recent advances in inorganic 2D materials and their applications in lithium and sodium batteries, J. Mater. Chem. A 5 (8) (2017) 3735–3758.
[80] M.A. Spackman, P.G. Byrom, A novel definition of a molecule in a crystal, Chem. Phys. Lett. 267 (3–4) (1997) 215–220.
[81] D. Li, et al., Modeling the SEI-formation on graphite electrodes in LiFePO4 batteries, J. Electrochem. Soc. 162 (6) (2015) A858.
[82] M.B. Pinson, M.Z. Bazant, Theory of SEI formation in rechargeable batteries: capacity fade, accelerated aging and lifetime prediction, J. Electrochem. Soc. 160 (2) (2012) A243.
[83] A. Smith, J. Burns, J. Dahn, A high precision study of the Coulombic efficiency of Li-ion batteries, Electrochem. Solid State Lett. 13 (12) (2010) A177.
[84] F.T. Krauss, I. Pantenburg, B. Roling, Transport of ions, Molecules, and electrons across the solid electrolyte Interphase: what is our current level of understanding? Adv. Mater. Interfac. 9 (8) (2022) 2101891.

[85] R. Malik, D. Burch, M. Bazant, G. Ceder, Particle size dependence of the ionic diffusivity, Nano Lett. 10 (10) (2010) 4123–4127.
[86] B. Balamurugan, I. Aruna, B.R. Mehta, S.M. Shivaprasad, Size-dependent conductivity-type inversion in Cu 2 O nanoparticles, Phys. Rev. B 69 (16) (2004) 165419.
[87] P.A. Bhatt, A. Pratap, P.K. Jha, Size and dimension dependent diffusion coefficients of SnO 2 nanoparticles, in: AIP Conference Proceedings, vol. 1536, American Institute of Physics, 2013, June, pp. 237–238, 1.